

Numerical Simulation of Mixed Convection Flows in a Square Double Lid-Driven Cavity Partially Heated Using Nanofluid

A. A. Abbasian Arani^{a,*}, J. Amani^a, M. Hemmat Esfeh^a

^a Mechanical Engineering Department, University of Kashan, Kashan, I.R. Iran

Article history:

Received 21/8/2012

Accepted 19/11/2012

Published online 1/12/2012

Keywords:

Non-uniform wall temperature

Partially heated

Double lid-driven cavity

Mixed convection

*Corresponding author:

E-mail address:

abbasian@kashanu.ac.ir

Phone: 98 361 5912413

Fax: +98 361 5912475

Abstract

A numerical study has been done through an Al_2O_3 -water in a double lid-driven square cavity with various inclination angles and discrete heat sources. The top and right moving walls are at low temperature. Half of the left and bottom walls are insulated and the temperatures of the other half are kept at high. A large number of simulations for a wide range of Richardson number of 0.1 to 10, Reynolds number from 1 to 100, inclination angle of cavity from -90° to 90° and solid volume fraction between 0 and 0.06 are performed. The results are presented in the form of streamline, isotherm and Nusselt number plots. The influence of solid volume fraction of nanofluids and angle of inclination on hydrodynamic and thermal characteristics have been analyzed and discussed. As a result, it was found that the heat transfer increases with increase in solid volume fraction for a constant Reynolds number, heat transfer also increases with increase in Richardson and Reynolds for a particular volume fraction.

2012 JNS All rights reserved

1. Introduction

Fluid flow and heat transfer in a cavity which is driven by buoyancy and shear force are encountered in a variety of thermal engineering applications [1–3]. Interaction of buoyancy force due to temperature gradient and forced convection due to shear forces is a complex phenomenon in mixed convection flow and heat transfer. Numerous research on this type of problem including the single or double lid-driven cavity flow and heat transfer involving different

cavity configurations, various fluids and imposed temperature gradients have been published in the last two decade. For example, Sharif [4] conducted a study for laminar mixed convection in shallow inclined driven cavities with hot moving lid on top and cooled from bottom and concluded that the average Nusselt number increases with cavity inclination angle for forced convection-dominated regime ($\text{Ri}=0.1$) while it increases much more rapidly for natural convection-dominated regime

($Ri=10$). Kandaswamy et al. [5] conducted a numerical study on buoyancy-driven convection in a cavity with partially thermally active vertical walls. They showed that heat transfer rate is increased when the heating location is at middle of the hot wall. Ghasemi and Aminossadati [6] made a numerical study on mixed convection in a partially heated square cavity. In this study, they kept the right wall at low temperature and move vertically either a constant velocity or with a sinusoidal oscillation. The results indicated that the direction and magnitude of the sliding wall velocity affect the heat transfer rate. In most of the studies found in the literature, vertical walls are considered to be isothermal in mixed convection flow and heat transfer in cavity. However, in many engineering applications, angle of cavity and the heater and cooler play an important role in the fluid flow and heat transfer, particularly for electronic equipment cooling. In order to understand the effect of cavity inclination and heater size and locations on mixed convection, in the present study we examine the heat transfer and fluid flow for a different model of this type of problem in a lid-driven cavity.

In addition, all of cited above studies were done for a pure base fluid without nanoparticles. Nanofluids are a new class of fluid consist a suspension of nanometer-sized particles (below than 100 nm) in a base fluid such as water, ethylene glycol or propylene glycol. Use of high thermal conductivity metallic nanoparticles increases the thermal conductivity of such mixtures [7]. Nanofluid caused an enhancement in thermal performance and a motivation for generation and using this new heat transfer fluid in building heating, in heat exchangers, in plants and in automotive cooling applications. Therefore in two last two decade, nanofluids have attracted more attention for using as coolant (working fluid) in various industrial applications. For

instance just 0.3% volume fraction of copper nanoparticles with 10 nm diameter led to an increase of up to 40% in the thermal conductivity of ethylene glycol [8].

By a literature survey one can found that a few studies have been done on mixed convection in a lid-driven cavity for a nanofluid. Muthamilselvan et al. [9] studied the heat transfer enhancement of copper-water nanofluids in a lid-driven enclosure with different aspect ratios and solid volume fraction. They confirmed that the addition of Cu nanoparticles into pure water increased the thermal performance of the cavity. Recently Abbasian Arani et al. [10] present a numerical study on mixed convection in a cavity. They conducted an investigation on the effects of Richardson number, phase deviation of sinusoidal heating, and volume fraction of nanoparticles on flow and temperature field.

It must be pointed that the heat transfer enhancement by using of nanofluids is still a controversial issue. Ho et al. [11] and Abu-Nada [12] argued that the augmentation or mitigation of heat transfer reported in the published numerical studies is due to the variation in the models used to predict the properties of nanofluids. Thus, further Computational Fluid Dynamics (CFD) studies need to take account of more accurate modeling of nanofluid properties.

This study deals with the mixed convection heating of nanofluid in a square enclosure where the bottom and left walls are heated non-uniformly, right and top walls are cooled and pulled with a uniform velocity. These boundary conditions are typical representations of heating of fluid in a container where heat treatment is applied at the bottom and the side wall would correspond to non-uniform heating rate such that the heating rate is zero at a portion of the bottom and left walls. The cold side wall often appears in presence of cold outer environment and this cold side wall may also cause locally larger

thermal gradient. Convection patterns in such situation may be interesting and the studies on mixed convection with such boundary conditions are not yet reported till date. The aim of the present investigation is to provide a complete understanding about the physical insight of the problem, solution procedure using finite volume method and detailed analysis of temperature and the flow fields on heat transfer evaluation.

2. Mathematical Model

The schematic diagram of current study is displayed in Fig. 1.

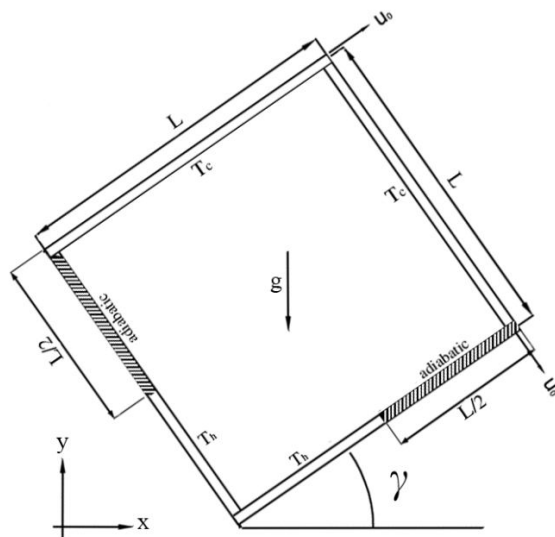


Fig. 1 Schematic diagram of the physical system.

It basically consists of a double-lid driven square cavity with side L filled with Al₂O₃-water nanofluid where the shape and size of solid particles are assumed to be uniform. It assumes that the nanofluid in the cavity is Newtonian, incompressible and laminar. The half of left and bottom walls maintain at high temperature, T_h. The top and right walls of the cavity are assumed to move in its own plane with a constant velocity, U₀, and at low temperature, T_c, that T_c is lower than T_h. Other portions of walls are adiabatic.

With this configuration and boundary conditions, the present investigation has done for the cavities at inclination angles range from -90° to 90°, Richardson number from 0.1 to 10 and Reynolds number between 1 and 100. The impact of mentioned above parameters on the streamline, isotherms and the average Nusselt number is discussed. It is assumed that the Boussinesq approximation is valid for body force term. Thermophysical properties of base fluid and particles are given in table 1.

Table 1. Thermophysical properties of base fluid and nanoparticles [8].

Physical Properties	Fluid (Water)	Solid (Al ₂ O ₃)
Cp(J/kg K)	4179	765
ρ (kg/m ³)	997.1	3970
K (W m ⁻¹ K ⁻¹)	0.6	25
β×10 ⁻⁵ (1/K)	21.	0.85
μ×10 ⁻⁴ (Kg/m s)	8.9

The governing equations are mass, momentum and energy. These equations are converted to non-dimensional form by using the non-dimensional variable that normally used in this type of problem. For density, thermal capacity and thermal expansion of nanofluid general relation for mixture are used. Thermal diffusivity, viscosity and conductivity of nanofluid are expressed as bellow:

$$\alpha_{nf} = \frac{k_{nf}}{(\rho c_p)_{nf}}, \quad \mu_{nf} = \frac{\mu_f}{(1-\phi)^{2.5}} \tag{1}$$

$$\frac{k_{nf}}{k_f} = \frac{k_s + 2k_f - 2\phi(k_f - k_s)}{k_s + 2k_f + \phi(k_f - k_s)} \tag{2}$$

The viscosity of the nanofluid expressed by the Brinkman [13] and the effective thermal conductivity of the nanofluid approximated by the Maxwell–Garnetts model [14].

The dimensionless forms of governing equations are as follows:

$$\frac{\partial U}{\partial X} + \frac{\partial V}{\partial Y} = 0 \tag{3}$$

$$U \frac{\partial U}{\partial X} + V \frac{\partial U}{\partial Y} = -\frac{\partial P}{\partial X} + \frac{\nu_{nf}}{\nu_f} \frac{1}{Re} \nabla^2 U + \frac{Ri}{Pr} \frac{\beta_{nf}}{\beta_f} \theta \sin \gamma \tag{4}$$

$$U \frac{\partial V}{\partial X} + V \frac{\partial V}{\partial Y} = -\frac{\partial P}{\partial Y} + \frac{\nu_{nf}}{\nu_f} \frac{1}{Re} \nabla^2 V + \frac{Ri}{Pr} \frac{\beta_{nf}}{\beta_f} \theta \cos \gamma \tag{5}$$

$$U \frac{\partial \theta}{\partial X} + V \frac{\partial \theta}{\partial Y} = \frac{\alpha_{nf}}{\alpha_f} \nabla^2 \theta \tag{6}$$

In order to investigation the heat transfer enhancement, the local Nusselt number defined as Eq. (7):

$$Nu = \frac{hL}{k_f} \tag{7}$$

The average Nusselt number are calculated over the hot surfaces by Eq. (8) by assuming a continuum surface of two heat source surfaces. Each heat source length is equals to $L/2$. The total hot surface length is L . The parameter ‘ l ’ indicates the differential length in direction of heat source surface.

$$Nu_m = \frac{1}{L} \int_0^L Nu dl \tag{8}$$

The boundary conditions are in the following forms:

$$\text{Right wall: } \begin{cases} U = 0, & V = -U_0 \\ \theta = 0 \end{cases} \tag{9}$$

$$\text{Left wall: } \begin{cases} U = 0, & V = 0 \\ \theta = 1, & 0 < Y \leq \frac{1}{2} \\ \frac{\partial \theta}{\partial X} \Big|_{x=0} = 0, & \frac{1}{2} < Y < 1 \end{cases} \tag{10}$$

$$\text{Bottom wall: } \begin{cases} U = 0, & V = 0 \\ \theta = 1, & 0 < X \leq \frac{1}{2} \\ \frac{\partial \theta}{\partial Y} \Big|_{y=0} = 0, & \frac{1}{2} < X < 1 \end{cases} \tag{11}$$

$$\text{Top wall: } \begin{cases} U = U_0, & V = 0 \\ \theta = 0 \end{cases} \tag{12}$$

3. Numerical method

Numerical solutions to the governing equations carry out by use the finite volume computational procedure and the SIMPLE algorithm as given in Patankar [15]. The present numerical solution was

validated by comparing the present code results and results of Basak et al. [1].

There is accordance between diagrams according to Fig. 2.

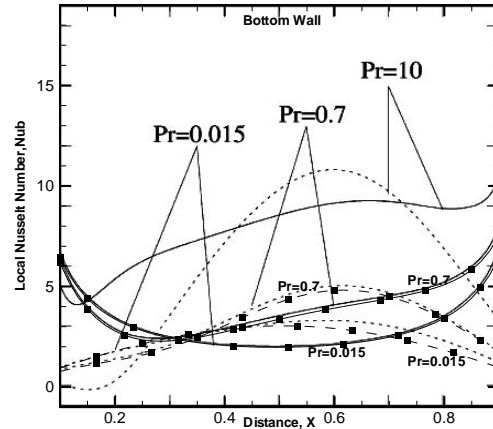


Fig. 2. Local Nusselt numbers for current study (---) and Basak (....) [1].

Numerical code was tested for grid independence by calculating the average Nusselt number on the heat source surface according to table 2 for two different cases. It was found that a grid size of 151×151 ensures a grid independent solution in uniform mesh.

Table 2. Mesh finding.

Grid	Average Nusselt Number and Ψ_{max} for			
	$\gamma = 0^\circ, \phi = 0.06, Re = 10, Ri = 5$		$\gamma = 60^\circ, \phi = 0.0, Re = 100, Ri = 1$	
	\overline{Nu}_m	Ψ_{max}	\overline{Nu}_m	Ψ_{max}
25×25	3.2272	0.1788	5.8607	0.1621
41×41	3.3178	0.1763	5.8558	0.1609
65×65	3.3798	0.1747	5.8929	0.1605
91×91	3.4037	0.1742	5.9340	0.1604
111×111	3.4180	0.1739	5.9553	0.1603
133×133	3.4283	0.1737	5.9724	0.1603
151×151	3.4363	0.1736	5.9827	0.1603
171×171	3.4395	0.1736	5.9859	0.1603
191×191	3.4405	0.1736	5.9871	0.1603

4. Results and discussion

Investigations through the cavity are made for the ranges of the Richardson number from 0.1 to 10. Reynolds number and nanoparticle concentration varies between 1 to 100 and 0.0 to 0.06 respectively. Cavity angle has a value of range -90 to 90 degree. Figs. 3-8 represent the isotherms and streamlines for Richardson equal to 3 and nanoparticles concentration between 0.0 and 0.06. In all cases, with increasing Reynolds number, intensity of the streamlines and temperatures near hot walls increases and stronger circulation appears in the cavity. So the flow rate near surfaces increases and consequently the total heat transfer increases. Different behavior is observed by change of the Reynolds number. Buoyancy force at $\gamma = -90^\circ$ (Fig. 3) is minimum and movement of hot flow due to buoyancy force is in the same direction so that only a clockwise circulation is generated in the cavity. Only one circulation is observed in the cavity with the increasing of γ to 30° (Fig. 3 and 4) because buoyancy and shear forces are in same direction. At $\gamma = 30^\circ$ to $\gamma = 90^\circ$, Fig. 4 and 5, buoyancy force generates a counterclockwise circulation.

Since the movement of the walls generates CW circulation in the cavity, at high Reynolds numbers in which two above-mentioned forces become important, two circulations are generated in the cavity. The strength and the dimension of circulations near the hot walls increase by enhancement of γ or Reynolds number. The buoyancy forces at $\gamma = 0^\circ$ and $\gamma = 90^\circ$ are the same but shear force opposes buoyancy force in $\gamma = 90^\circ$. Thus Nu_m for $\gamma = 0^\circ$ is more than $\gamma = 90^\circ$.

By increasing of γ from -90° to -30° , Fig. 3, the streamlines become more intensified near the surfaces. An opposite behavior is observed at $\gamma = 0, 30$ and 60 degrees, Fig. 4. Temperature lines change

for $\gamma = 90^\circ$, Fig. 8, at high Reynolds number because of the formation of two circulations in the cavity.

In Fig. 7 it is clearly observed that intensity of temperature lines for $\gamma = 90^\circ$ is higher than $\gamma = 60^\circ$. Buoyancy force increases by enhancement of angle from -90° to -30° . At these angles, buoyancy and shear forces are in the same direction. Thus it is expected that Nu_m increases by increasing of γ from -90° to -30° .

The bottom surface of heat source has more effect on heat transfer at $\gamma = -30^\circ$ relative to $\gamma = 0^\circ$. Also, upward movement of hot flows due to buoyancy force affects the temperature lines and streamlines near the left heat source (vertical wall), Fig. 6 and 7. Thus Nu_m for $\gamma = -30^\circ$ is more than Nu_m for $\gamma = 0^\circ$. As mentioned, the average Nusselt number decreases for angles from 0° to 60° . The dimension of circulation increases for $\gamma = 90^\circ$, Fig. 5, due to clash of two moving flows created by heat transfer and lids wall. This circulation covers about half of the cavity. So for $\gamma = 90^\circ$, Nu_m is more than that of $\gamma = 60^\circ$ in $Ri = 7$ and 10. At $Ri = 3$ and 0.1, Nu_m decreases by increasing of angles because the contribution made by the natural heat transfer is lower than force convection.

In all angles with increasing of Richardson number, Fig. 9 the contribution of forced convection to the buoyancy force reduces. At angles in which the buoyancy force and shear force in the same direction, with increasing Richardson number, a stronger flow field is created in the cavity. Also temperature gradient near the heat source surfaces increases and so does the amount of heat transfer. But at angles that both buoyancy force and shear force neutralize each other, Nu_m is reduced by increasing of Richardson number.

As it is shown in Fig. by increasing of Richardson from streamlines become closer to walls and thus stronger circulation is generated in the cavity. These

behaviors created by the interaction of the above mentioned forces observed.

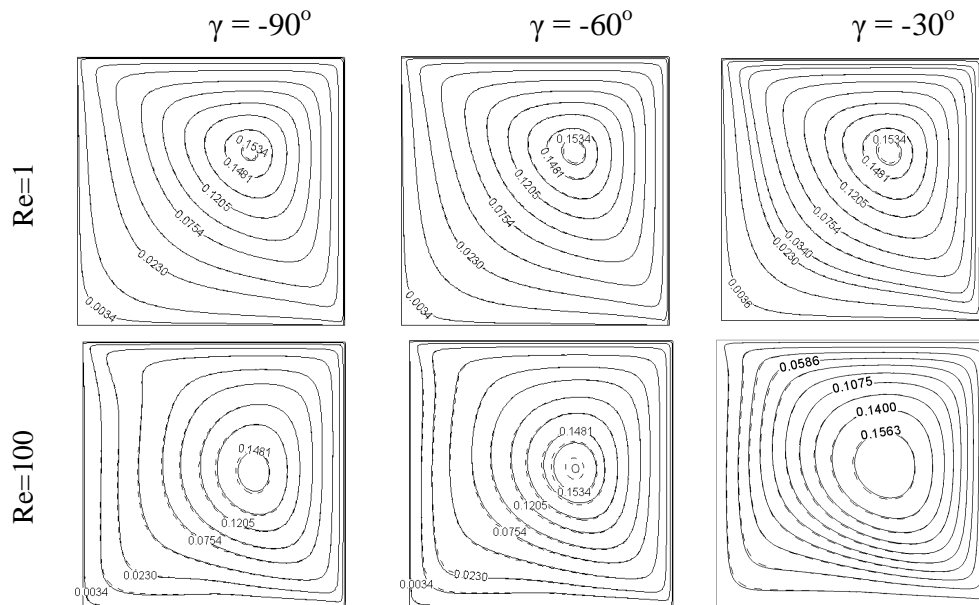


Fig. 3. Stream function for partially heated side walls with inclination angle between -90 and -30 and Reynolds numbers equal to 1 and 100 at Richardson number 3.

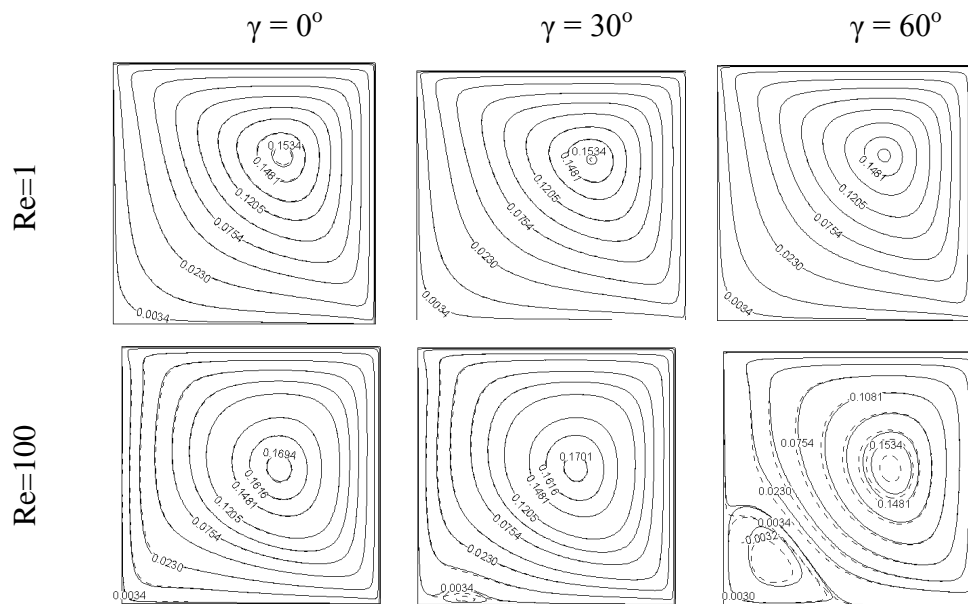


Fig. 4. Stream function for partially heated side walls with inclination angle between 0 and 60 and Reynolds numbers equal to 1 and 100 at Richardson number 3.

Isotherms depict some curves whose center is in the left corner for Richardson=1. When Richardson increases to 10, isotherms are closer to each other

near the hot surfaces and total heat transfer augments due to the enhancement of temperature gradient near the hot walls. The average Nusselt number diagrams

are given in Fig. 10 for $\gamma = -60^\circ$. It is observed that Nu_m increases by the increment of Reynolds number and nanoparticle concentration. Also enhancement in Richardson number results in enhancement of Nu_m . Fig. 11 shows Nu_m for all cases under study at Richardson from 0.1 to 10, Reynolds number between 1 and 100 versus angle of inclination and solid volume fraction from 0.0 to 0.6. The Nu_m increases by increasing of solid volume fraction for all cases under study. While the cavity inclination varies, Nu_m changes as mentioned. This change is

very small for $Ri=0.1$, Figs 11b, d, h, because in this case forced convection is dominate and angle of inclination dose not effect on average Nusselt number. The value of average Nusselt number increases by increasing the Reynolds number from 1 to 100 in these cases, about 400%. Same situation has been occurs for Reynolds number equal to 1 for all Richardson number under study, Figs 11a, b, and 11e, f. The value of average Nusselt number is constant versus angle of inclination and Richardson number.

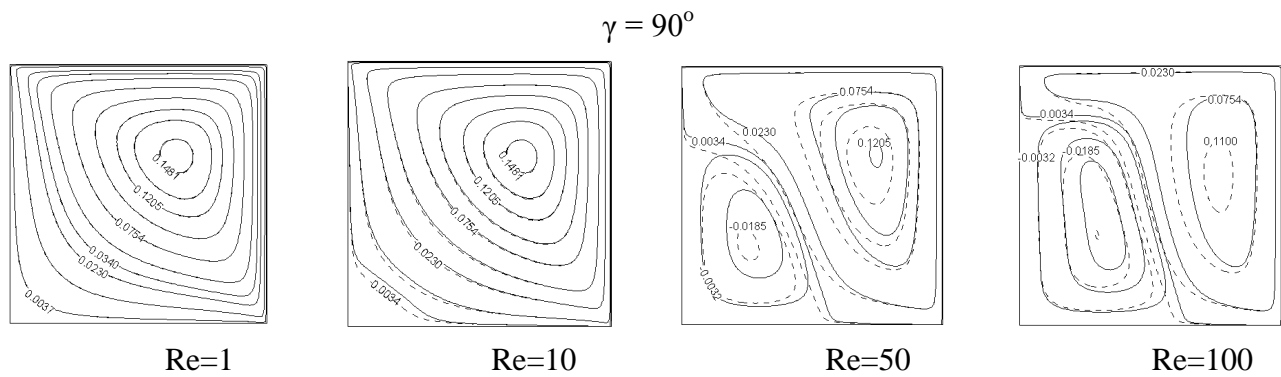


Fig. 5. Stream function for partially heated side walls with inclination angle 90 and Reynolds numbers from 1 to 100 at Richardson number 3.

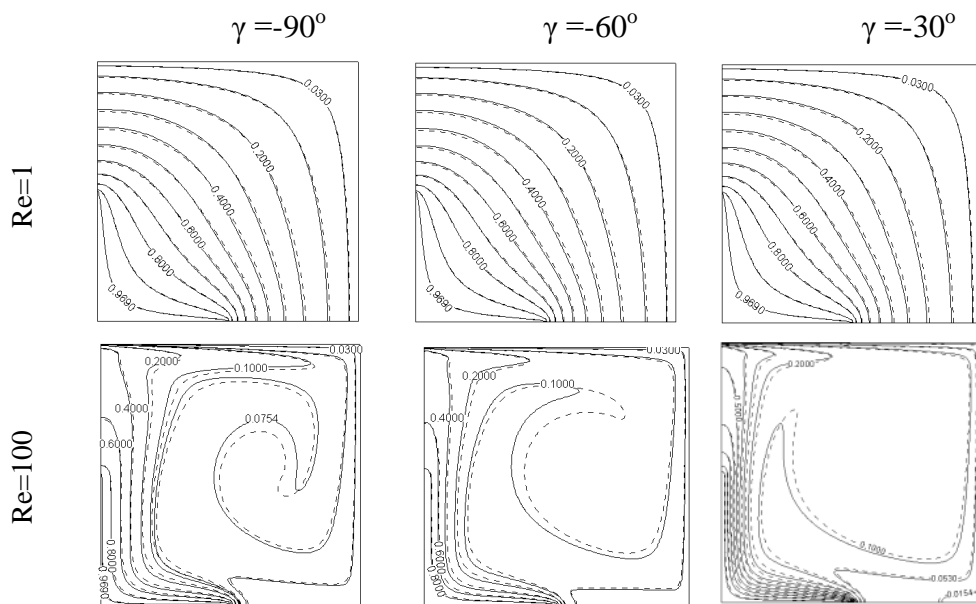


Fig. 6. Temperature contours for partially heated side walls with inclination angle between -90 and -30 and Reynolds numbers equal to 1 and 100 at Richardson number 3.

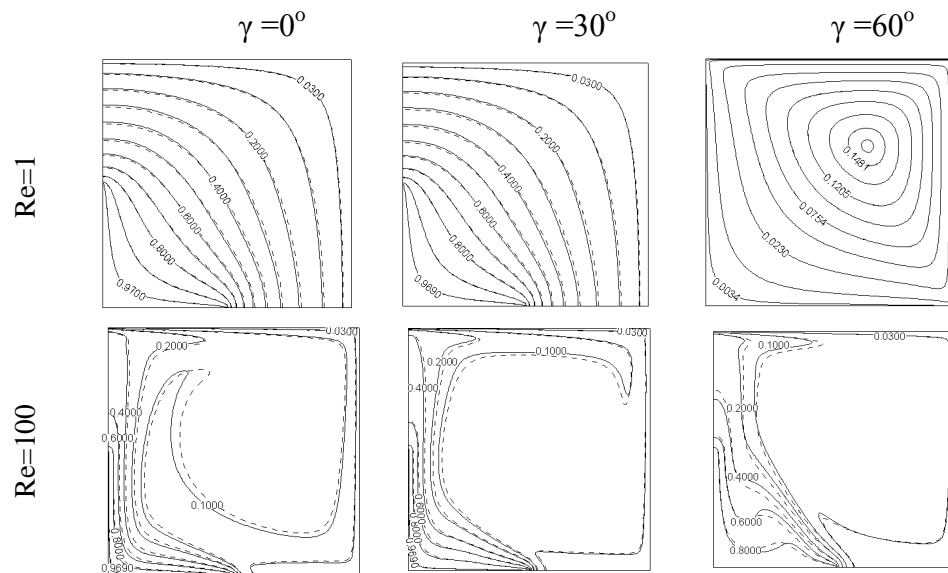


Fig. 7. Temperature contours for partially heated side walls with inclination angle between 0 and 60 and Reynolds numbers equal to 1 and 100 at Richardson number 3.

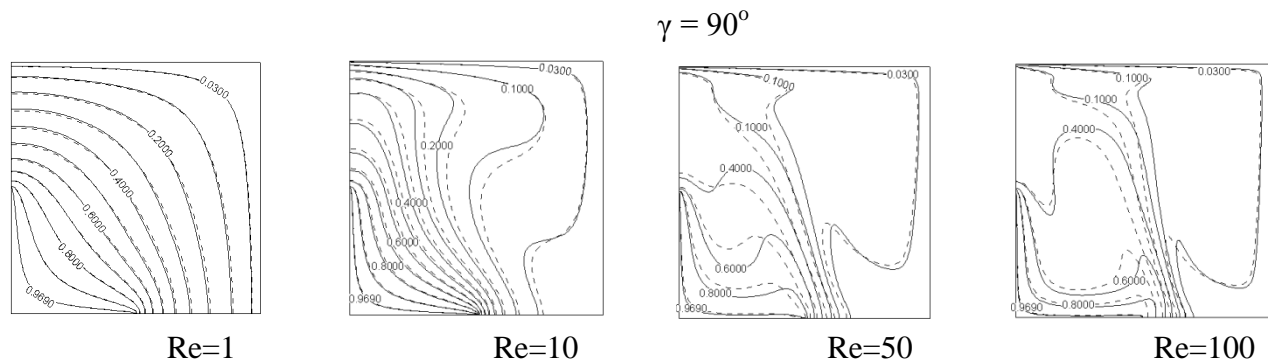


Fig. 8. Temperature contours for partially heated side walls with inclination angle 90 and Reynolds numbers from 1 to 100 at Richardson number 3.

In this situation natural convection is dominant and for this type of boundary condition (constant temperature on bottom and left walls) change of inclination angle has no effects on natural convection. In addition Reynolds number is low, then shear force is small and when this force is opposite to Buoyancy force, it has no effect on total Nusselt number.

For Reynolds number equal to 10, 50 and 100, Nu_m increases by increasing of inclination angle from -90°

to -30° , Fig 11c, g, f, and k. By changing of inclination angle from -30° to 0° and then to 60° , as mentioned, Nu_m reduces. Then by enhancement of inclination angle to 90° , Nu_m decreases for Richardson number equal to 3 and increases/decreases for Richardson number equal to 7 and 10. As natural convection is lower than forced convection, Nu_m reduces at these angles at Richardson as 0.1 or 3.

5. Conclusion

This work focused on mixed convection (combined forced and natural convection) through an Al_2O_3 -water in a double lid-driven square cavity with various inclination angles and discrete heat sources. In this study a number of simulations for a wide range of the controlling parameters consist of Richardson number, Reynolds number, inclination angle of cavity, and solid volume fraction were performed.

The results are presented in the form of streamline, isotherm and Nusselt number plots. The Nu_m increases by increase of solid volume fraction for all

cases under study. At low Reynolds numbers or low Richardson number, Nu_m variations are very small and don't change for some cases at all. The value of average Nusselt number increases by increasing the Reynolds number from 1 to 100 at $Ri=0.1$, about 400%. For Reynolds number equal to 10, 50 and 100, Nu_m increases by increasing of inclination angle from -90° to -30° . By changing of inclination angle from -30° to 0° and then to 60° , as mentioned, Nu_m reduces. Then by enhancement of inclination angle to 90° , Nu_m decreases for Richardson equal to 3 and increases/decreases for Richardson number equal to 7 and 10.

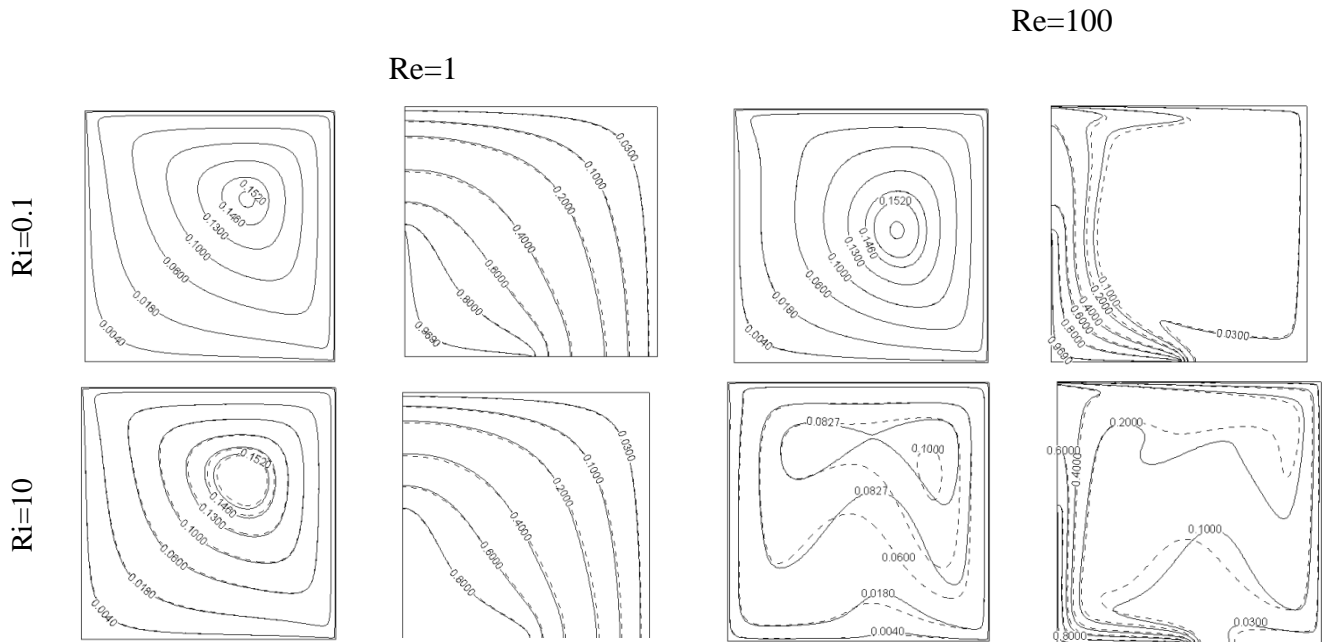


Fig. 9. Stream function and temperature contours for partially heated side walls with inclination angle 30, Reynolds number 1 and 10 and Richardson number equal to 0.1 and 10.

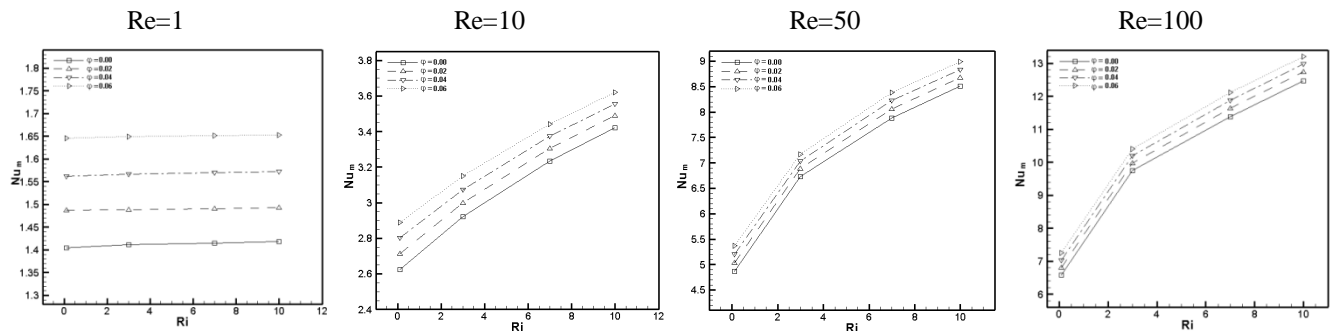


Fig. 10. Average Nusselt number at $\gamma = -60^\circ$ for various nanoparticles concentration versus Richardson number.

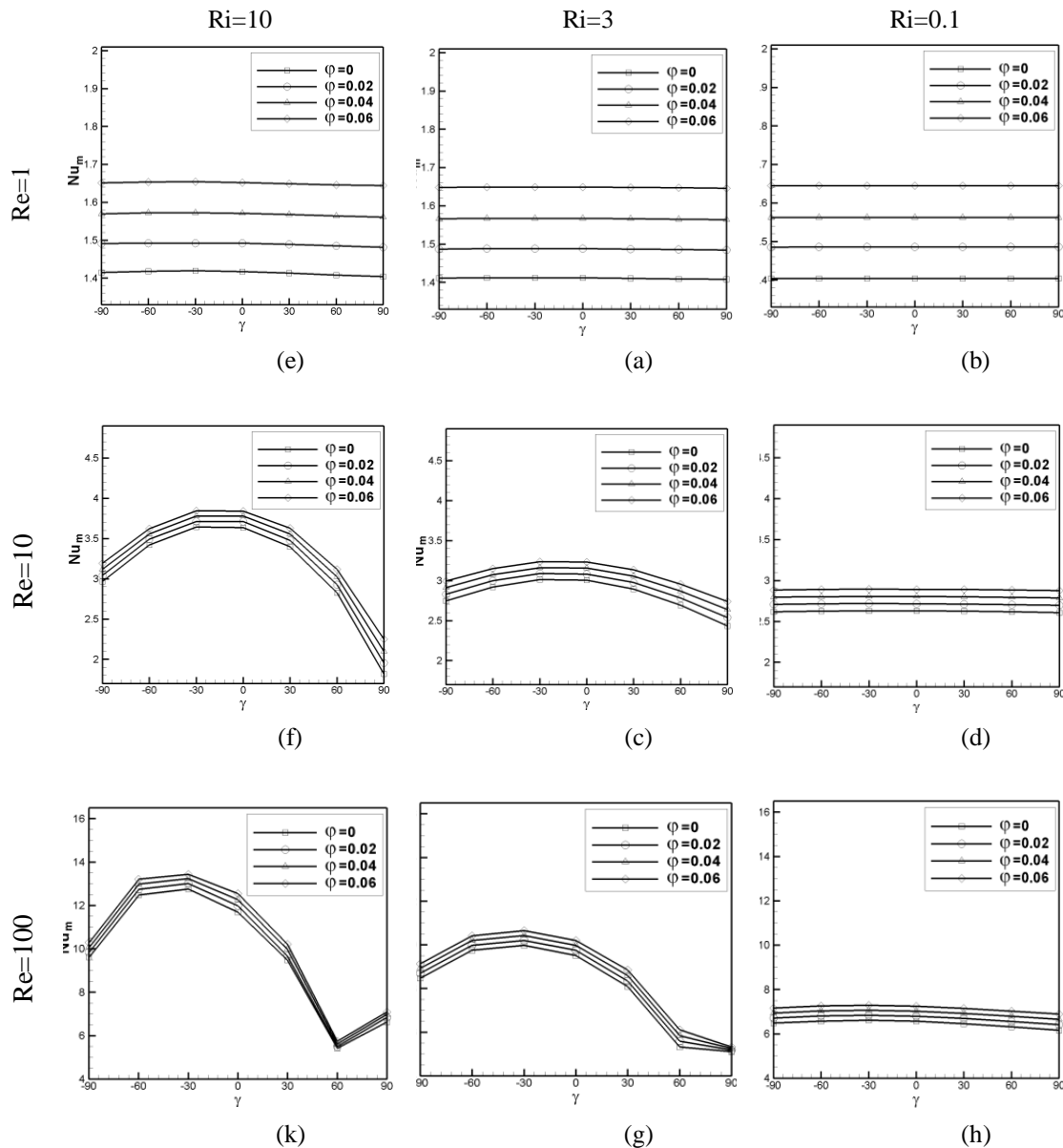


Fig. 12. Average Nusselt number at Richardson number 0.1 and 3, for Reynolds number from 1 to 100 versus inclination angle.

Acknowledgments

The authors would like to thank the referees for their valuable comments. The authors are grateful to University of Kashan for supporting this work by Grant No. 158506. They would also like to thank the

Iranian Nanotechnology Development Committee for their financial support.

Nomenclature

c_p	specific heat, $J\ kg^{-1}\ K^{-1}$
g	gravitational acceleration, $m\ s^{-2}$
h	heat transfer coefficient, $W\ m^{-2}\ K^{-1}$

k	thermal conductivity, $\text{W m}^{-1} \text{K}^{-1}$
L	cavity height and width, m
Nu	Nusselt number
p	pressure, N m^{-2}
P	dimensionless pressure
Pr	Prandtl number
q	heat flux, W m^{-2}
Ra	Rayleigh number
Re	Reynolds number
Ri	Richardson number
T	dimensional temperature, K
u, v	dimensional velocities components in x and y direction, m s^{-1}
U, V	dimensionless velocities components in X and Y direction
U_0	lid velocity
x, y	dimensional Cartesian coordinates, m
X, Y	dimensionless Cartesian coordinates

Greek symbols

α	thermal diffusivity, $\text{m}^2 \text{s}$
β	thermal expansion coefficient, K^{-1}
θ	dimensionless temperature
μ	dynamic viscosity, $\text{kg m}^{-1} \text{s}$
ν	kinematic viscosity, $\text{m}^2 \text{s}$
ρ	density, kg m^{-3}
ϕ	volume fraction of the nanoparticles
γ	Inclination angle

Subscripts

c	cold
f	fluid
h	hot
h	hot
m	average
s	solid particles
w	wall

References

- [1] T. Basak, S. Roy, P.K. Sharma, I. Pop, *Int. J. Therm. Sci.* 48 (2009) 891–912.
- [2] G. Guo, M.A.R. Sharif, *Int. J. Therm. Sci.* 43 (2004) 465–475.
- [3] R.K. Tiwari, M.K. Das, *Int. J. Heat Mass Trans.* 50 (2007) 2002–2018.
- [4] M.A.R. Sharif, *Appl. Therm. Eng.* 27 (2007) 1036–1042.
- [5] P. Kandaswamy, S. Sivasankaran, N. Nithyadevi, *Int. J. Heat Mass Trans.* 50 (2007) 942–948.
- [6] B. Ghasemi, S.M. Aminossadati, *Num. Heat Trans. Part A* 54 (2008) 726–743.
- [7] Y. Xuan, Q. Li, *J. Heat Trans.* 125 (2003) 151–155.
- [8] S. Choi, *ASME Publications* 66 (1995) 99–105.
- [9] M. Muthamilselvan, P. Kandaswamy, J. Lee, *Commun. Nonlinear Sci. Num. Simulation.* 15 (6) (2010), 1501–1510.
- [10] A.A. Abbasian Arani, S. Mazrouei Sebdani, M. Mahmoodi, A. Ardeshiri, M. Aliakbari, *Superlattices and Microstructures* 51 (6) (2012) 893–911.
- [11] C.J. Ho, M.W. Chen, Z.W. Li, *Int. J. Heat Mass Trans.* 51 (17–18) (2008) 4506–4516.
- [12] E. Abu-Nada, *Int. J. Heat Fluid Flow* 30 (4) (2009) 679–690.
- [13] H.C. Brinkman, *J. Chem. Phys.* 20 (1952) 571–581.
- [14] J. Maxwell, *A Treatise on Electricity and Magnetism*, second ed. Oxford University Press, Cambridge, UK, 1904.
- [15] S.V. Patankar, *Numerical Heat Transfer and Fluid Flow*, Hemisphere Pub. Co., Washington, DC, 1980.